TECHNISCHE MECHANIK
an open access journal

journal homepage: www.ovgu.de/techmech

Tech. Mech., Vol. 40, Is. 2, (2020), 134–148

Received: 04.02.2020
Accepted: 26.03.2020
Available online: 06.04.2020

A study on harmonic excitation based experimental characterization of damping materials for acoustic simulations

Lars Spannan[1]*, Fabian Duvigneau[1], Maria Gavila Lloret[2], Christian Daniel[1], Daniel Juhre[1], and Elmar Woschke[1]

[1] Otto-von-Guericke University, Institute of Mechanics, Universitätsplatz 2, 39106 Magdeburg, Germany
[2] BMW AG, Knorrstraße 147, 80788 München, Germany

Abstract: The presented study deals with the experimental characterization of damping materials for acoustic simulations with respect to the stiffness and damping in dependence of the excitation frequency, i.e. frequency-dependent elasticity modulus. The test rigs under consideration utilize a shaker, acceleration sensors and a laser Doppler vibrometer (LDV) to measure oscillating behaviour at frequencies ranging from 20 to 2000 Hz. Suitable mounting properties of the test rigs are examined experimentally and by finite element analysis. The applicability of the gained results for acoustic simulations is investigated with results from a window test setup.

Keywords: foam, damping, stiffness, characterization, acoustics

1 Introduction

During the last years, the reduction of sound transmission towards the passengers cabin in automobiles gained importance in order to improve the driving experience and customer satisfaction. Beside the reduction of noise sources, passive elements such as damping layers are widely used to lower the level of noise transmitted to the passengers. In order to assess the choice of material, structure and geometry for such elements in the early development stages, simulative approaches are striven for. Such simulation approaches were already developed, for example, for a holistic consideration of engines by Duvigneau et al. (2016). The main difficulty of all numerical analyses in acoustics is an accurate modelling of the vibroacoustic properties of the damping materials, which are used in almost every real world application that presents acoustic issues. A proper modelling of damping materials is also of utmost importance if innovative materials, such as acoustic metamaterials (Duvigneau and Duczek (2017)), are under investigation to find an optimal design for the given task.
Experimental methods are used to determine the material properties required for the models used in the acoustic simulations. The main assumption for a macroscopic description of the dynamic behaviour assumes homogenized material properties, often in combination with isotropic and linear media.
The skeleton of polymeric poroelastic materials, such as polyurethane foams frequently used in the automotive industry for acoustic treatment, have a viscoelastic behaviour. This means that under deformation the material exhibits viscous as well as elastic characteristics (Lakes (1998)). For the typical deformation amplitudes that noise control treatments undergo, the behaviour remains in the linear viscoelastic regime. Additionally, in the present study we assume isotropic material behaviour. Unlike elastic materials, the loading and unloading paths for a viscoelastic material are not the same. The dissipated energy per cycle inside the material due to viscoelastic losses is known as hysteresis loss.
The methods for the characterization of the elastic parameters can be classified in three groups (Renault (2008)). First, there are approaches based on the velocity at which waves propagate inside the poroelastic material. For instance, the velocity of the Rayleigh waves can be related to the shear modulus G and the Poisson ratio ν of the material (Allard et al. (2002); Boeckx et al. (2005)). In order to identify these, a layer of poroelastic material is fixed to a rigid plate on one of its ends. On the other end, the layer is excited with a harmonic signal through a shaker. A laser vibrometer is employed to measure the displacement on the surface. The fitting of the theoretical and the measured phase velocities delivers frequency-dependent values for G and ν. In order to calculate the theoretical solution, the poromechanical parameters need to be determined beforehand, which is a cumbersome and expensive process. The method utilized in this paper does not need the identification of the poromechanical parameters in advance.
In the second kind of characterization methods, the shear modulus and the Poisson ratio are calculated with the help of acoustic methods. A material sample with rigid backing is excited by a monopoly source. A microphone located near the sample measures the pressure resulting from the direct and the reflected fields. After that, the poroelastic material is replaced by a rigid, impervious surface and the procedure is repeated. The ratio between the two pressures is then calculated. Again, from the contrast between the obtained values and the theoretical solution, provided that the poromechanical parameters are known, the elastic parameters G and ν can be derived, see Allard et al. (2005).
The third group is formed by the vibrational methods, which are based on the response of the material subjected to mechanical excitation. The vibrational approaches are further broken down into two categories: The quasi-static methods, in which the inertial effects are neglected, and the dynamic techniques, which include them. In the quasi-static compression approach proposed by Langlois et al. (2001) two material samples of different shape factor are measured. The shape factor is defined as the ratio

* E-mail address: lars.spannan@ovgu.de
doi: 10.24352/UB.OVGU-2020-021

of half the radius to the thickness of a cylindrical sample. After that, several finite element simulations on elastic solids under compression are run to obtain polynomial relations that link the measured compression stiffness to the elasticity modulus, the Poisson's ratio and the shape factor. In order to account for the inertial effects, this setup can be modified to conduct a dynamic uni-axial compression, like the configuration presented by Pritz (1986, 1994).
A review of other quasi-static and dynamic experimental methods, including torsion and shear loading can be found in Renault (2008) and Jaouen et al. (2008). In the scope of Gavila Lloret (2018) six different poroelastic foams were analysed following these methods. It can be noted that the values of the elasticity modulus obtained with the quasi-static compression method (Langlois et al. (2001)) are systematically lower than the ones provided by the dynamic method (Pritz (1986)) since the former neglects the inertial effects. As the frequency increases, the inertial force increases and gets significant in comparison to the elastic force in the system, see Koblar and Boltežar (2016). Therefore the utilization of dynamic characterization techniques becomes necessary.
As already mentioned, the dynamic behaviour of the solid skeleton is viscoelastic and frequency-dependent. Rigobert et al. (2004) and Van der Kelen et al. (2014) give two examples on the modelling of a poroelastic layer that covers a structurally excited plate. In both cases the foam layer was described using the full poroelastic formulation. It was first found that the application of the quasi-static elastic parameters resulted in a poor comparability with the experimental data. In a second step, a frequency-dependent profile for the elastic properties was defined by fitting the calculated predictions to the reference data sets. Even if this derivation leads to a good prediction of the vibroacoustic behaviour, it presents the great disadvantage that a measurement of the complete setup is first needed in order to obtain the frequency-dependent parameters. At this point, we address presentable measurement methods that follow a simple and robust approach, while the number of material parameters remains low and parameters without physical interpretation are renounced. In addition, the measurement of the complete experimental setup for model-updating purposes is undesired. In such cases the advantages of numerical simulations would be lost.
The theory of poroelasticity by Biot (1956a,b); Allard and Daigle (1994) is the state of the art in numerical modelling of poroelastic media. Its main underlying assumption is the homogenization. This means that, provided that the lengths of the waves propagating inside the material are much larger than the pore size, the biphasic aggregate can be considered as a homogeneous medium in which the two phases are simultaneously present. Consequently, the resolution of the pores on the micro scale is avoided. The two governing equations have the form of a fluid-structure interaction problem with the particularity that the mechanical coupling between the elastic frame deformation and the fluid behaviour is not limited to the fluid structure interfaces, but is of a volume nature. The coefficients of the equation can be grouped into three classes - fluid properties, elastic and poromechanical parameters. The first set includes the material properties of the filling fluid, namely its density, its viscosity and the speed of sound. The elastic parameters characterize the response of the frame in vacuum and are typically the Young's modulus, the Poisson ratio, the structural damping coefficient and the density of the drained material. The poromechanical parameters help to link the microscopic thermal and viscous effects at a local level with the changes in the macroscopic effective bulk modulus and effective dynamic density. This requires a constitutive model as, for example, the one proposed by Johnson et al. (1987), Champoux and Allard (1991) (JCA), which is employed as reference for the conducted numerical simulation in section 4.1. Some procedures to determine the values of these mentioned material parameters can be found in Jaouen et al. (2008); Salissou and Panneton (2007); Atalla and Panneton (2005).
An alternative to the complex poroelastic modelling is the simplification of the material as an elastic solid. This approach has the major advantage of avoiding the characterization of the poromechanical parameters, which is a laborious task and requires specific test equipment. However, since the presence of the fluid phase is neglected, some dissipation mechanisms inside the poroelastic medium may not be correctly represented, especially at high frequencies. In particular, if constant elastic material parameters are used, large differences at higher frequencies occur as presented by Van der Kelen et al. (2014).
An option to include the missing mechanisms is to condense the additional effects by means of frequency-dependent elastic parameters, which is pursued in the paper at hand. The frequency-dependent characterization of poroelastic materials, which is carried out analogously to classical viscoelastic media, was also utilized by Cuenca et al. (2014) and Finnveden et al. (2014). An experimental setup to determine frequency-dependent elasticity modulus and Poisson ratio based on sine burst excitation is proposed by Bonfiglio and Pompoli (2015). One general trend that can be identified is an increasing elasticity modulus with frequency. This is a common progression for polymers and other viscoelastic materials, which do not have a crystalline structure (Sfaoui (1995); Ferry (1980)). Since the frame of the investigated polyurethane foams is also a viscoelastic material, such a frequency behaviour is to be expected. In comparison to poroelastic models it needs less (exclusively physical) parameters, which are easier to interpret and can be identified in parallel with the same experimental setup. Moreover, poroelastic models do not work properly for foams with closed cells as closed pores are neglected in the sense that they are counted as part of the solid structure (Pride and Berryman (1998)). Finally, the material modelling within the numerical simulation is also straightforward beside causing fewer degrees of freedom.
In the following section two experimental methods are described and frequency-dependent complex elasticity moduli are derived. The limits of the methods and influences arising from the boundary conditions are discussed. Regarding the latter, the choice of lightweight but sufficiently stiff bearings, which load the foam samples, is investigated experimentally and by finite element analysis. Different designs and arrangements of the test set-up are presented and their advantages and disadvantages are evaluated in order to determine a preferred variant for engineering practice. Section 3 sums up the measurement results of the frequency-dependent elasticity moduli of two structurally different foams gained from the final measurement setup. The determination of the material properties gets more challenging with higher excitation frequencies due to the required energy, therefore the testing frequency ranges from 20 to 2000 Hz. Section 4 presents a window test rig and the associated acoustic simulation model in which the applicability of the presented characterization method is examined. In section 5 a conclusion and an outlook are given.

Tab. 1: Specimen overview of two foams of bright (B) and dark (D) colour with edge lengths of 30 mm and 50 mm or diameters of 30 mm, respectively. Specimen duplicates are enumerated by x.

Label	Color	Width W [mm]	Length L [mm]	Height H [mm]
B□50.x	bright	50	50	15.8
B□30.x	bright	30	30	15.8
D□50.x	dark	50	50	10.25
D□30.x	dark	30	30	10.25
Label	Color	Diameter D [mm]		Height H [mm]
B○30.x	bright	30		15.8
D○30.x	dark	30		10.25

Fig. 1: Viscoelastic representation of the material behaviour (left) and foam samples B□50.x (center) and D○30.x (right).

2 Experimental methods

Different experimental methods have been presented in the literature in order to characterize frequency-dependent stiffness and damping behaviour of poroelastic media. A comprehensive study with a focus on reproducibility of the approaches was conducted by several researchers and is published by Bonfiglio et al. (2018), also depicting the challenges. Referring to the literature review given in the introduction we focus on the third group of characterization methods, namely the vibrational methods. Especially, we exclusively consider dynamical methods, as from our point of view the frequency dependency of the material properties is of utmost importance. Consequently, quasi-static methods are not sufficient for this purpose.
In the study at hand, two methods are investigated out of which the material properties are derived. The applied material model is viscoelastic with a frequency-dependent stiffness parameter $c(f)$ and damping parameter $d(f)$, Fig. 1. This characteristic can be represented independently of the specimen geometry by using the apparent complex elasticity modulus E:

$$E(f) = E'(f) + i\,\bar{E}(f) = c(f)\frac{H}{A} + i\,2\pi f d(f)\frac{H}{A}\,. \tag{1}$$

With f, H, A being the frequency under consideration, the foam sample height and the foam surface area under load, respectively. Due to the assumption of constant Poisson ratio in the presented procedures, the given elasticity modulus is an apparent value. A comparison of the results obtained from the measuring methods will be given in section 3, including a discussion on sources of deviations and the influence parameters, as for example the boundary conditions.
Two open cell polyurethane molded foam products with different mechanical properties are considered. For the ease of distinctiveness their colour is used for labelling within this article. One foam is of bright colour and one is of dark colour, identified in the following sections by the characters ”B” and ”D”, respectively. Geometric specifications of the used specimens are summarized in Tab. 1. To verify the reproducibility, multiple specimens of the foam samples were analysed. In general, we used three specimens per specification.

2.1 Resonance Method

The first method utilized represents a suspended mass with support node excitation in vertical direction. Located between two steel plates, the specimen is modelled with a linear spring and a linear damper element connected in parallel, see Fig. 2. The lower mass m_a represents the masses of the movable parts of the shaker, the base plate and the acceleration sensor 1. The mass m_s includes the suspended masses of the top mass and the acceleration sensor 2. The mass of the specimen is equally distributed to the two entities, m_a and m_s. With the assumption of sole vertical movement, the set-up represents a damped oscillator with one degree of freedom with the eigenfrequency of

$$f_0 = \frac{1}{2\pi}\sqrt{\frac{c(f_0)}{m_s}} \tag{2}$$

and the damping factor

$$D = \frac{d(f_0)}{c(f_0)}\pi f_0\,. \tag{3}$$

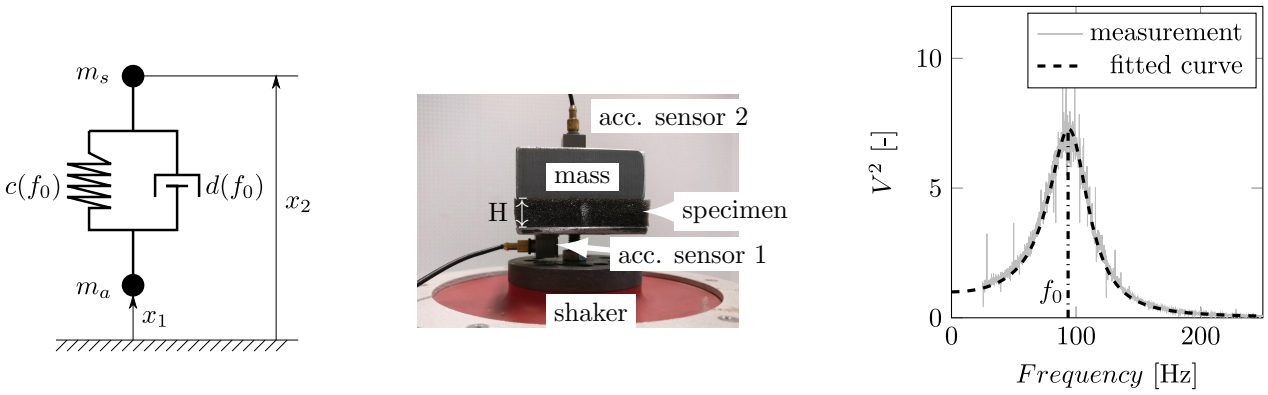

a) Mechanical model b) Vertical test rig c) Resulting squared transfer function

Fig. 2: Resonance measurement arrangement.

The shaker excites with a white Gaussian noise signal that results in a broadband excitation. The acceleration of the base plate $\ddot{x}_1$ and the response of the top mass $\ddot{x}_2$ are simultaneously measured. Subsequently, the resulting transfer function V of the Fourier transformations $\mathcal{F}(\ddot{x}_1)$ and $\mathcal{F}(\ddot{x}_2)$ can be fitted to the analytical solution of the one dimensional oscillator model (Nashif et al. (1985))

$$V(\eta, D) = \frac{\mathcal{F}(\ddot{x}_2)}{\mathcal{F}(\ddot{x}_1)} = \frac{\sqrt{1 + 4D^2\eta^2}}{\sqrt{(1-\eta^2)^2 + 4D^2\eta^2}} \tag{4}$$

or the squared form

$$V^2(\eta, D) = \frac{1 + 4D^2\eta^2}{(1-\eta^2)^2 + 4D^2\eta^2}\,, \tag{5}$$

respectively, with $\eta = f/f_0$ being the tuning ratio. Eq. 5 is fitted to the measured data in a least-square sense in order to obtain the resonance frequency f_0 and the dimensionless damping factor D as presented in Fig. 2 c). Taking into account the specimen height H and the orthogonal face area A, the viscoelastic behaviour can also be reformulated as the real part E' and imaginary part $\bar{E}$ of the complex elasticity modulus, according to Eqs. (1), (2) and (3)

$$E'(f_0) = 4\pi^2 f_0^2\, m_s\, \frac{H}{A}, \tag{6}$$

$$\bar{E}(f_0, D) = 2\, D\, E'. \tag{7}$$

In order to obtain a frequency-dependent description of the material behaviour, the procedure has to be carried out with different top masses m_s to realize different resonance frequencies. With a view on acoustics applications, this method is limited regarding high frequencies requiring lightweight top masses, which are prone to detach from the specimen.

2.1.1 Measurement Results

As noted above, the major drawback of the method presented in Sec. 2.1 is the relatively low maximum testing frequency because of the limitation in the weight of the top masses. The presented foams with edge lengths of 50 mm were tested with weights ranging from 67 g to 418 g, resulting in a resonance frequency range from 33 Hz to 181 Hz, which is hardly relevant for acoustical problems. The calculated real and imaginary parts of the elasticity modulus according to Eq. (6) and Eq. (7) are summarized in Tab. 2 and depicted in Fig. 3. The results show good repeatability and an increase in stiffness with frequency. This is particularly evident for the bright foam. The specified standard deviation results from eight measurements with one for each possible orientation of the foam. One cause of deviation may arise due to the imperfections in the foam structure, as can be seen in Fig. 1.
In an attempt to expand the frequency range by utilizing adhesive tape and strong fast-acting adhesives in order to prevent detachment, a significant influence on the stiffness and damping results was identified, see Tab. 2 variations a) and b). With the help of the adhesives the detachment of the 71 g mass could be prevented, but the two adhesive modifications led to significantly different results. Additionally, with higher excitation amplitudes, referenced as condition c), the top mass can separate, which causes deviations of the resulting stiffness. The positioning of the acceleration sensors, condition d), also gives rise to variations in the results due to non strict one dimensional movement. Therefore, a centred positioning of the sensors is advised in order to minimize the influence due to tilting motion of the masses. Furthermore, it cannot be ruled out that the resulting viscoelastic properties may be influenced by the pre-compression or the compression rate of the foam during the experiment due to the variation of the top load. Due to the limited frequency range, investigations with the resonance method were discontinued and further investigations regarding the influences mentioned above were not conducted.

Tab. 2: Tests with the resonance procedure and modifications of the boundary conditions. -) Standard configuration. a) Using adhesive tape. b) Using strong fast-acting adhesive. c) High excitation amplitude. d) Sensors not centered. The specified bounds represent standard deviations resulting from eight repetitions, one for each different orientation.

Spec.	cond.	m_s [g]	f_0 [Hz]	E' [kN/m²]	$\bar{E}$ [kN/m²]
D□50.1	-	418	74.49 ± 0.71	375.52 ± 7.21	46.26 ± 4.63
D□50.2	-	357	78.41 ± 0.83	355.79 ± 7.48	43.24 ± 1.37
D□50.3	-	357	80.57 ± 1.07	375.61 ± 10.09	46.85 ± 6.46
D□50.1	-	211	103.36 ± 1.06	342.55 ± 61.49	40.75 ± 7.23
D□50.1	a)	71	181.02 ± 7.96	375.21 ± 32.54	75.01 ± 1.27
D□50.1	b)	71	159.96 ± 2.53	292.65 ± 9.23	49.90 ± 1.18
D□50.1	b), d)	71	144.19 ± 0.24	237.74 ± 0.80	44.83 ± 0.50
B□50.2	-	357	33.20 ± 4.27	99.38 ± 25.49	34.94 ± 8.66
B□50.1	-	110	77.12 ± 0.80	162.89 ± 3.35	68.92 ± 1.20
B□50.1	-	89	96.81 ± 2.23	207.88 ± 9.58	81.07 ± 9.94
B□50.1	-	71	100.32 ± 5.55	177.91 ± 20.29	86.66 ± 17.08
B□50.1	c)	71	69.04 ± 3.27	84.16 ± 8.00	56.78 ± 5.52
B□50.2	c)	71	96.05 ± 1.76	162.66 ± 5.95	97.53 ± 3.82
B□50.2	-	67	102.51 ± 1.31	174.79 ± 4.46	72.99 ± 1.44
B□50.3	-	67	97.60 ± 1.05	158.44 ± 3.41	68.04 ± 1.73

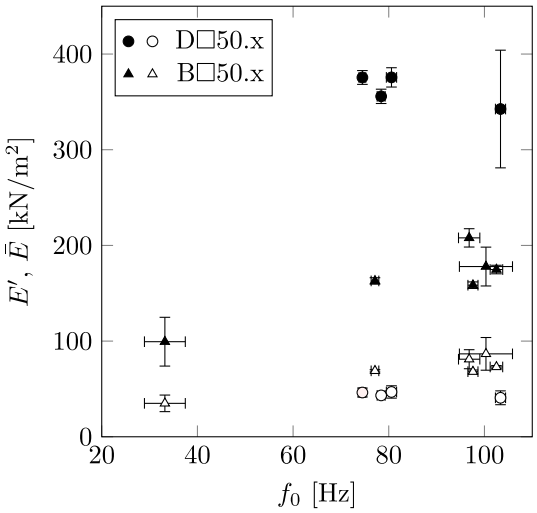

Fig. 3: Real (E', black marker) and imaginary ($\bar{E}$, white marker) parts of the elasticity moduli measured for the dark (D, round marker) and bright (B, triangular marker) foam samples in standard configuration without adhesives. The error bars represent the bounds specified in Tab. 2.

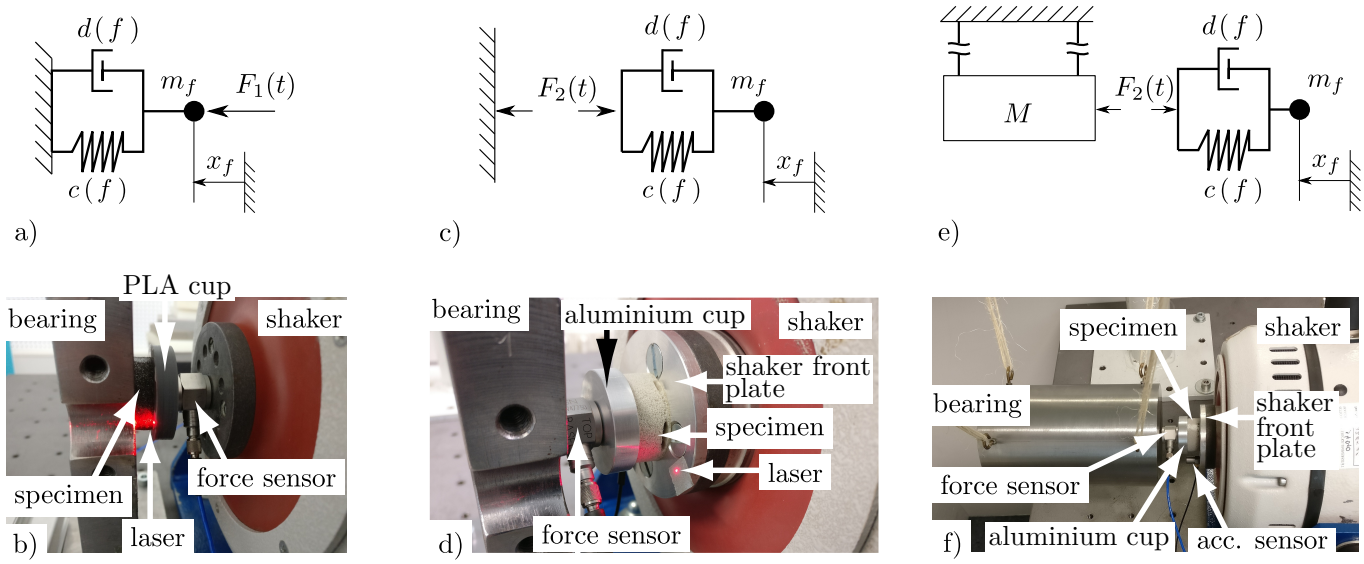

Fig. 4: Horizontal measurement arrangements. Shaker facing force sensor position: a) Mechanical model. b) Test rig. Bearing facing force sensor position: c) Mechanical model. d) Test rig. Seismic mass bearing: e) Mechanical model. f) Test rig.

2.2 Harmonic loading method

For the second characterization method, the specimen is horizontally aligned between the shaker and a bearing, which is assumed to be rigid. Different arrangements for the bearing have been investigated, as displayed in Fig. 4. The configurations in Fig. 4 a)-d) include a fixed bearing, but with different order of the specimen and the force sensor in the load path. In the setup in Fig. 4 e)-f) a seismic mass bearing hangs in a free-free boundary condition. The shaker provides a harmonic force F that loads the specimen at a frequency f.
A laser Doppler vibrometer (LDV) is utilized to measure the deflection x_f. After a few oscillations, the steady state is reached and the periodic solution

$$x_f(t) = \check{x}_f \sin(2\pi f t + \psi) \tag{8}$$

with amplitude $\check{x}_f$ and phase ψ remains. For the setup in Fig. 4 e)-f) using the seismic mass bearing, the acceleration

$$\ddot{x}_f(t) = \check{\ddot{x}}_f \sin(2\pi f t + \psi) = -4\pi^2 f^2 \check{x}_f \sin(2\pi f t + \psi) \tag{9}$$

is measured with an appropriate acceleration sensor due to the lack of optical access for the LDV. The deflection amplitude is calculated by

$$\check{x}_f = \check{\ddot{x}}_f (-4\pi^2 f^2)^{-1} . \tag{10}$$

The approach with an acceleration sensor turned out to be just as feasible as the displacement measurement with the LDV. Again, the porous medium is modelled with a linear spring-damper combination with one single degree of freedom. This leads to the following balance of forces

$$F_1(t) = c\, x_f + d\, \dot{x}_f + m_f\, \ddot{x}_f \tag{11}$$

in the case where the force sensor is positioned between the shaker and the specimen, see Fig. 4 a). The mass m_f combines the weight of the adapter plate and partial contributions by the force sensor and the specimen. The determination of the latter two is prone to errors. Combining Eq. (8) and Eq. (11), the inertial force can be obtained as second derivative of the deflection signal with respect to time. The calculated inertial force is subtracted from the force signal to obtain the loading force $\bar{F}$ acting on the foam

$$\bar{F} = F_1(t) - m_f\, \ddot{x}_f(t) = c\, x_f(t) + d\, \dot{x}_f(t). \tag{12}$$

Due to the error-prone determination of the inertial component, this approach has a lower accuracy than the setup, where the force sensor is mounted between the specimen and the bearing. In the latter cases, Fig. 4 c)-f), inertial forces are not recorded by the force sensor and the compliance of the foam is assumed to be dominant, leading to

$$\bar{F} = F_2(t) = c\, x_f(t) + d\, \dot{x}_f(t). \tag{13}$$

The theoretical force-deflection diagram according to Eq. (13) yields an elliptical hysteresis curve which is met by the experimental data quite well, Fig. 5. The hysteresis loss W_D can be calculated with the integral of the foam loading force with respect to the load path

$$W_D = \oint \bar{F}\, \mathrm{d}x_f . \tag{14}$$

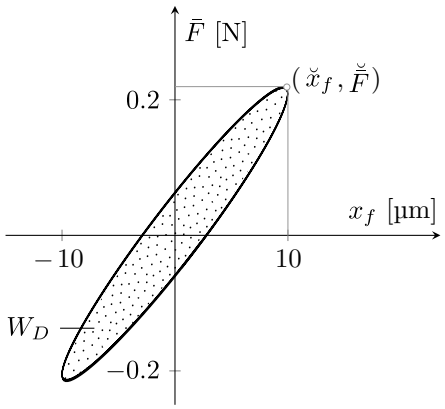

Fig. 5: Hysteresis loss of an example measurement of B○30.3 at 1100 Hz.

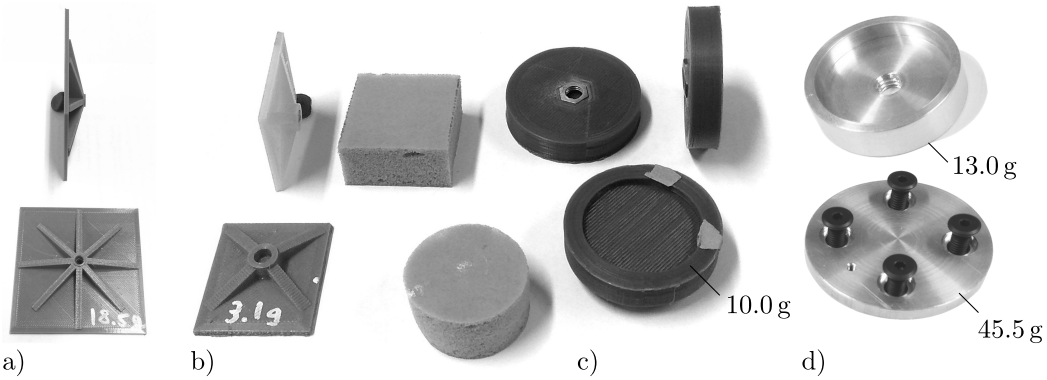

Fig. 6: Test setup iterations. a) PLA die with 70 mm edge length, 2 mm ground plate height and 18.5 g mass b) PLA die with 30mm edge length, 2 mm ground plate height and 3.1 g mass c) PLA die with 10.0 g mass for cylindrical probes of 30 mm diameter d) final design with aluminium cup (top) for 30 mm diameter probes and shaker front plate (bottom).

According to Eqs. (8) and (13), the stiffness and damping coefficients for the particular loading frequency f is gained by

$$c(f) = \frac{\breve{\bar{F}}}{\breve{x}_f}, \tag{15}$$

$$d(f) = \frac{W_D}{\breve{x}_f^2\, 2\pi^2 f}\,. \tag{16}$$

Recalling Eq. (1), the real and imaginary part of the elasticity modulus are

$$E'(f) = c(f)\,\frac{H}{A} \tag{17}$$

$$\bar{E}(f) = \frac{W_D(f)}{\breve{x}_f^2\,\pi}\,\frac{H}{A}\,. \tag{18}$$

2.2.1 Test set-up optimization

The frequency range of the method described in Sec. 2.2 is limited by the power of the shaker, the mass to be moved and the specified displacement amplitude. Therefore, several mass reducing iterations of the set-up were investigated in order to maximize the frequency range without violating the assumption of a rigid set-up and dominant compliance due to the foam.
The first design with a square steel sheet with an edge length of 70 mm and a thickness of 0.75 mm showed evident flexibility during operation. In the first step, the steel sheet was replaced by a rapid prototyped die with an edge length of 70 mm and a ground plate height of 2 mm made of PLA (polylactide), depicted in Fig. 6 a). In order to test the assumption of rigidity, a smaller die with an edge length of 30 mm and a ground plate height of 2 mm was used to test the square foam specimens with 30 mm edge length, Fig. 6 b). Despite the benefit of higher frequency ranges, a comparison of the determined frequency-dependent elasticity moduli with the two PLA dies showed a significant discrepancy. For that reason, finite element analyses were carried out in order to evaluate the rigidity assumption of the PLA die from Fig. 6 b), which is less compliant because of the geometry.

Finite element analysis (FEA) evaluation

A finite element representation of the experimental setup was modelled to identify measurement deviations due to compliant components. The geometrical parameters and material properties used for the foam domain are specified in Tab. 3. Due to the

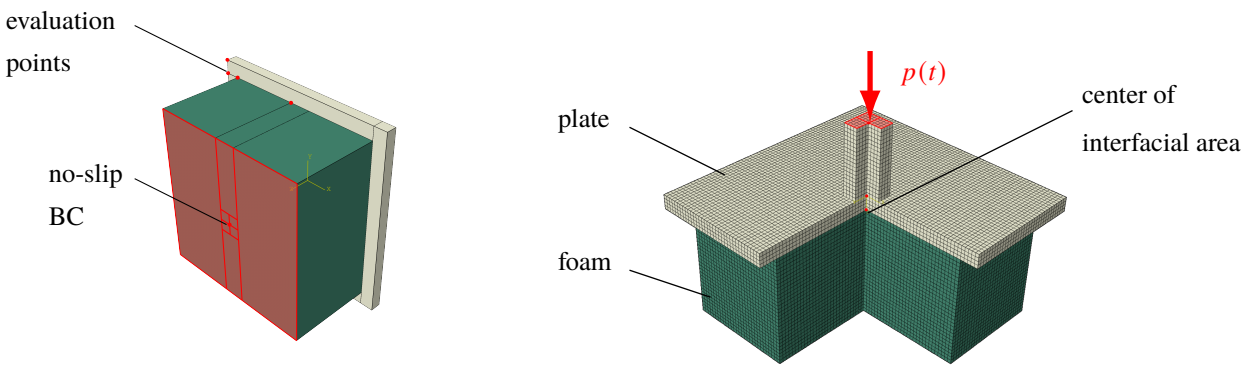

Fig. 7: Utilized grid in the finite element analysis.

Tab. 3: Isotropic elastic parameters and geometry of the foam domain in the FEA.

E'_{foam} [kN/m²]	ρ_{foam} [kg/m³]	ν_{foam} [−]	L_{foam} [mm]	B_{foam} [mm]	H_{foam} [mm]
5000	25.4	0.3	30	30	15.75

assumption of increased stiffness of the foam at higher frequencies the finite element analysis was carried out for a maximum anticipated elasticity modulus of $E'_{foam} = 5000\,\text{kN/m}^2$. The simulation parameters are summarized in Tab. 4. Fig. 7 shows the domain discretization as well as the load-controlled boundary conditions. According to Lerch et al. (2009) and the material data in Tab. 3, resonances may occur above the border frequencies

$$\frac{\sqrt{E'_{\text{foam}}(1-\nu)}}{\sqrt{\rho(1-\nu-2\nu^2)}\cdot 2\cdot \max(L,B,H)} \approx 8580\,\text{Hz}$$

for longitudinal wave propagation and

$$\frac{\sqrt{E'_{\text{foam}}}}{\sqrt{2\rho(1+\nu)}\cdot 2\cdot \max(L,B,H)} \approx 4586\,\text{Hz}$$

for transversal wave propagation, respectively. With a testing frequency of 500 Hz a sufficient gap to the critical values is kept.
In a first analysis, the die was modelled rigidly in order to compare the elasticity modulus derived from the force and deflection data to the input values, Tab. 3. With this analysis the suitability of the chosen boundary conditions, the time integration method, the excitation amplitude, the number of load cycles, the mesh discretization and the element type, see Tab. 4, was verified. A harmonic pressure load is applied at the square tip of a pin in the centre of the die, see Fig. 7, while the mesh is continuous at the boundary between the die domain and the foam domain. The deflection of all nodes on the opposite area of the foam domain is constrained in the load direction, whilst all three translational degrees of freedom of the central node of this face are constrained, too. As a consequence, contact formulations and possible gaps due to the axial movement are avoided in the interface area.
The analysis shows that the variation of the excitation amplitude, the number of load cycles, the load frequency and the foam elasticity modulus do not affect the results significantly. The derived elasticity modulus shows a deviation of approximately five percent with respect to the input value, which is considered sufficient. Inadequate discretization in time or mesh size can be identified not only by an increased deviation from the input value but also by hysteresis development in the force-deflection correlation, whilst material damping is not considered in the FE-model and a hysteresis is not to be expected.
The results of the FEA with a compliantly modelled die show a significant discrepancy to the rigid reference model, see Tab. 5, which is also evident when comparing the contour plots of the deflections in the loading direction in Fig. 8. The thickness of 2 mm for a plate shaped die of PLA material is not sufficient to fulfil the assumption of rigidity and the foam is loaded non-uniformly. The method can therefore be improved by choosing a die material with higher elasticity modulus or a stiffer geometry. Results of subsequent FE-models presented in Tab. 5 show that the compliance of the die in comparison to the foam gets negligible if the Young's modulus reaches values of the order of magnitude of steel or the thickness is increased to 6 mm. Aiming for a lightweight

Tab. 4: FEA simulation parameters.

Time integration	explicit, central diff.
Maximum time step size	8×10^{-5} s
Excitation amplitude	$1\,\text{N/mm}^2$
Deflection amplitude	$\approx 80\,\mu$m
Number of load cycles	10
Mesh factor (MF)	0.5 . . . 10
Maximum element size	$H_{\text{foam}}/(10\cdot\text{MF})$
Element type	linear hexahedrons

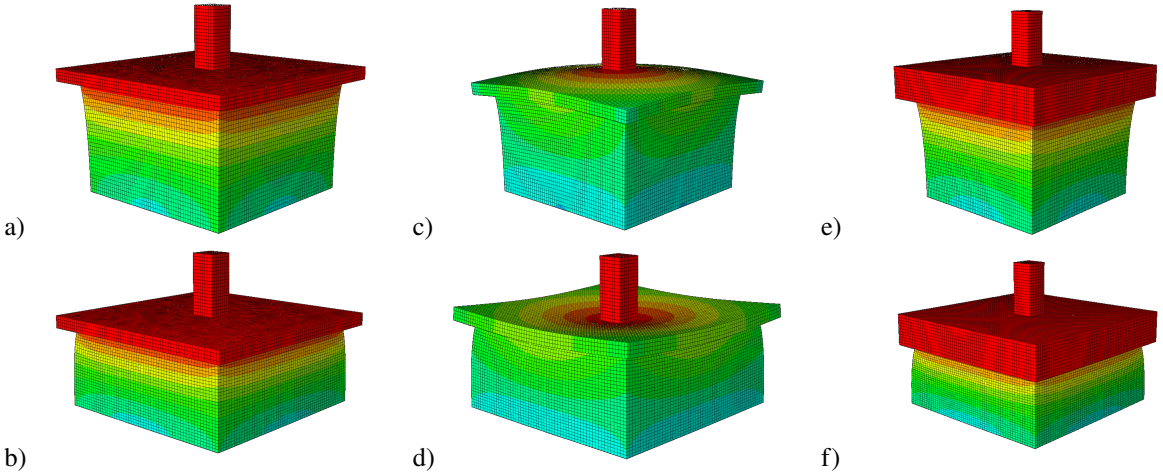

Fig. 8: FEA model deflections for different die properties. a),b) rigid die c),d) 2 mm thick die e),f) 6 mm thick die. Deflections are displayed with a scaling factor of 50.

Tab. 5: FEA results for an exemplary loading frequency of 500 Hz. Foam sample edge lengths are 30 mm. The center of the interfacial area is used for the evaluation.

E_{plate} [$^{\text{kN}}/_{\text{m}^2}$]	H_{plate} [mm]	H_{foam} [mm]	diff. to rigid [%]
5×10^6	2	15.75	29.43
50×10^6	2	15.75	7.81
210×10^6	2	15.75	4.79
5×10^6	6	15.75	5.08
5×10^6	2	20.0	25.61
5×10^6	2	30.0	19.31

structure, the increase of the PLA die height is favourable. Increasing the foam height also reduces the deviation, but undesirable lateral slip movements in the test bench are to be expected. In a following iteration, a hollow die with inner supporting structures, Fig. 6 c) is used to test round samples of foams with diameters of 30 mm. It was found that the used threaded connection to the shaker influenced the measurements detrimentally and despite the lower density of the PLA material, the use of aluminium parts result in a better stiffness to weight ratio. The final design consists of an aluminium plate shielding the shaker face and the force sensor mounted between the bearing and an aluminium cup, Fig. 4 d) and Fig. 6 d). The tested seismic mass bearing was not pursued further due to the cumbersome overall setup and adjustment of the initial compression of the foam at rest due to slow decay of the seismic mass swing motions. Under the assumption of a sufficiently stiff setup, the frequency-dependent properties were determined and the influence factors in the experimental process were investigated. The results are presented in the following section.

3 Measurement results

After discarding unsuitable setups and configurations, the preferred procedures were repeated with eight orientations of three foam samples for each foam material. Each facial area of the cylindrical samples is loaded four times while being unmounted and remounted with a 90° rotation along the loading axis between each measurement. This results in a total of 24 measurements for each material from which the standard deviation is calculated. All samples are cylindrical and the loading direction is always coinciding with the cylinder axis which matches the rising direction during manufacturing. The orientation also corresponds to the application direction of the acoustic treatment. The loading amplitude was specified with $\check{x} = 10\,\mu\text{m}$, which achieves a sufficient signal-to-noise ratio. The results shown below compare the derived parameters with those from the resonance method. An increase in the standard deviation of the gained results is evident for frequencies above 1200 Hz, especially for the bright foam. This may be a consequence of its inhomogeneous structure, which is visible in Fig. 1. Comparing both measurement methods presented, a good agreement at low frequencies near 100 Hz can be found for the imaginary part of the elasticity modulus for both foams, see Fig. 10, and for the real part of the elasticity modulus for the bright foam. In addition, Fig. 10 shows the associated damping loss factor underlining the good agreement of the mean value of both methods for the bright foam. Only the real part of the elasticity modulus of the dark foam shows considerable deviations between both measurement methods, see Fig. 9. This deviation may be caused by a significant dependence of the foam properties on the pre-load and compression rate due to the different top masses used in the resonance method leading to a higher elasticity modulus. This dependency seems to be less distinct for the bright foam. The undesired influence of the pre-load is inherent to the measuring principle of the resonance method whereas pre-compression and compression rate can be adjusted in the harmonic loading method.

Considering both parts of the elasticity modulus, a distinct frequency dependence in the stiffness and damping behaviour is evident from the gained results and needs to be considered in material models for the following numerical simulations. With respect to the gained results at 100 Hz, the real part of the elasticity modulus at 2000 Hz shows an increase by 275% for the bright foam and 62%

for the dark foam, respectively. The imaginary part of the elasticity modulus of the dark foam increases by 380% in the frequency domain ranging from 100 Hz to 2000 Hz. The imaginary part of the elasticity modulus of the bright foam varies between 66 $^{kN}/_{m^2}$ and 400 $^{kN}/_{m^2}$. The outlier for both foams at 700 Hz is linked to a resonance frequency in the test setup which should be resolved in future measurements as proposed in the outlook.

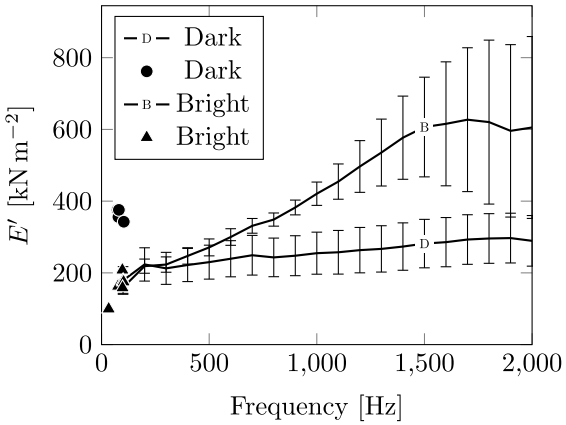

Fig. 9: Measurement results of the real part E' of the elasticity modulus of the bright (B) and dark (D) foam. Markers ● and ▲ represent results of the resonance method.

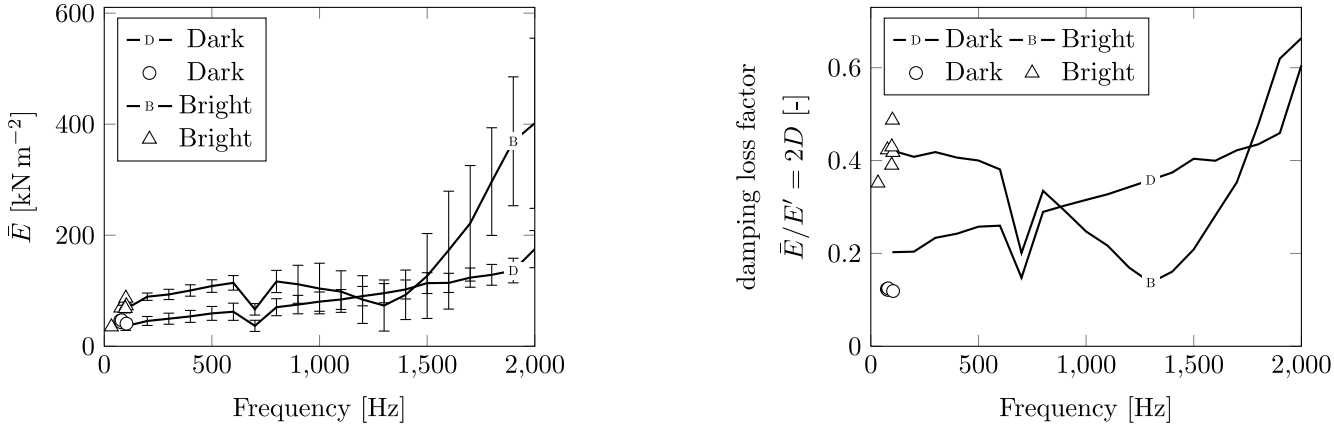

Fig. 10: Measurement results of the imaginary part $\bar{E}$ of the elasticity modulus (left) and the associated damping loss factor (right) of the bright (B) and dark (D) foam. Markers ○ and △ represent results of the resonance method.

3.1 Influence factors on the measurement results

Due to the manual arrangement of the shaker position, slight variations in the alignment of the foam sample in the test setup may occur. For this reason, a study on the influence of misalignments and the loading amplitude was conducted. Starting with the angular misalignment with respect to the loading plane, Fig. 11 a) and b), two additional measurements with noticeable misalignments were carried out. Again, the outlier at 700 Hz is attributable to a resonance frequency in the experimental setup. The data show that the deviation from the mean results is close to the standard deviation, although the misalignment is exaggerated and visible to the eye. A tendency of decreasing values for the real and imaginary part of the elasticity modulus is noticeable. Misalignments during a characterization procedure, which is executed with the necessary diligence, are much smaller than the extreme examples presented here and therefore considered tolerable. Consequently, the robustness of the presented method with regard to angular misalignment is shown.
Additionally, the manual positioning of the shaker relative to the bearing can result in longitudinal variances in the loading direction which can induce an initial compression of the foam. The initial loading must at least be larger than the loading amplitude in order to prevent a lift-off from the bearing or the shaker face-plate. If this requirement is fulfilled, the use of adhesives is unnecessary. Measurements with increasing initial compression of the foam sample were carried out and are presented in Fig. 12. It is evident that the real part as well as the imaginary part of the elasticity modulus decreases in the examined frequency range for both foams when the initial loading is increased. The maximum height reductions considered are 3 mm for the dark and 4.8 mm for the bright foam specimen, respectively. Considering that the initial loading paths are in the range of millimetres and that relative deviations of up to -35% may occur, this error must be reduced to a minimum. In order to achieve this, the shaker is carefully positioned and the initial foam thickness in the test bench is previously measured. It is assumed that only compressions of less than one millimetre occur during the regular measurements. As a result, a deviation of less than 10% is to be expected under the aspired avoidance of this influence. Conversely, the frequency dependence of the elasticity modulus is distinct and the results keep an advantage in comparison to the resonance characterization method, which only uses a few data points in the lower frequency domain.

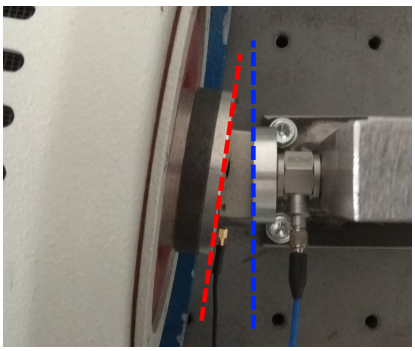

a) Top view

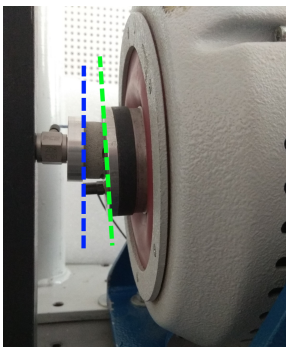

b) Side view

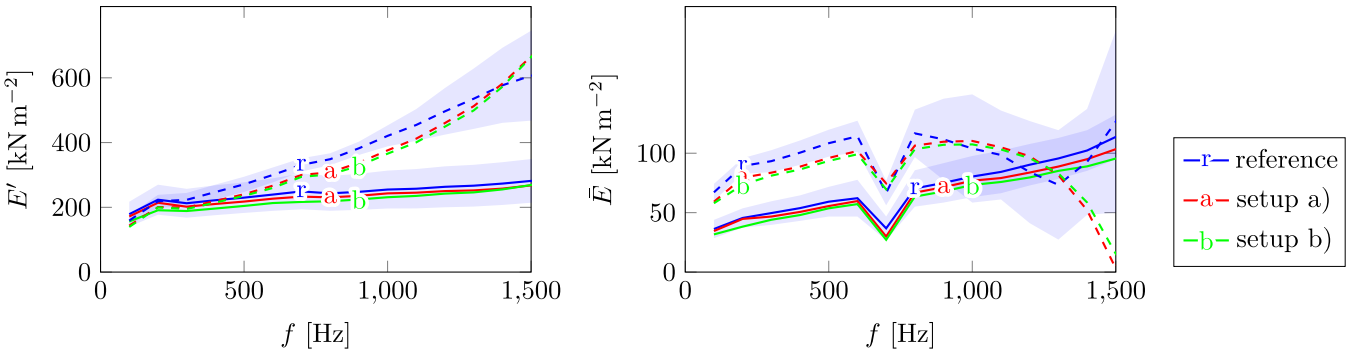

Fig. 11: Measurement with exaggerated misalignment of the foam loading. Solid lines: Dark foam. Dashed lines: Bright foam. The filled area represents the standard deviation from Fig. 9 and Fig. 10.

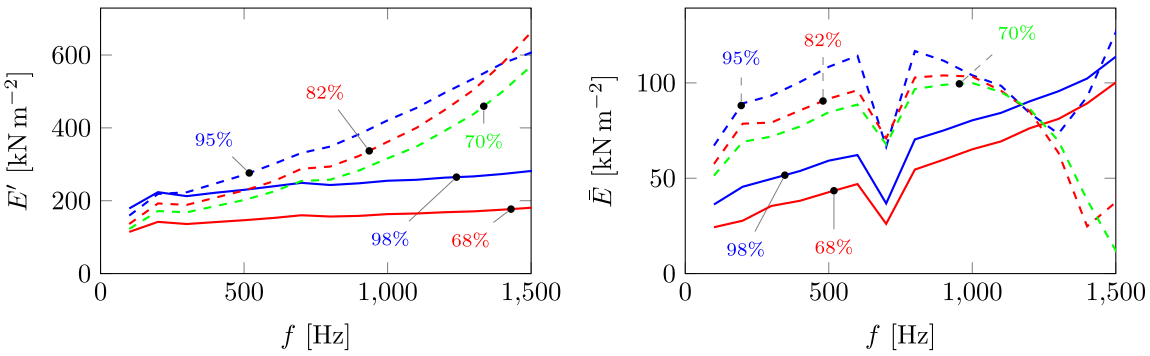

Fig. 12: Measurement with initial compression of the foam. Indicators represent the relative height with respect to the initial height of the foam samples. Solid lines: Dark foam. Dashed lines: Bright foam.

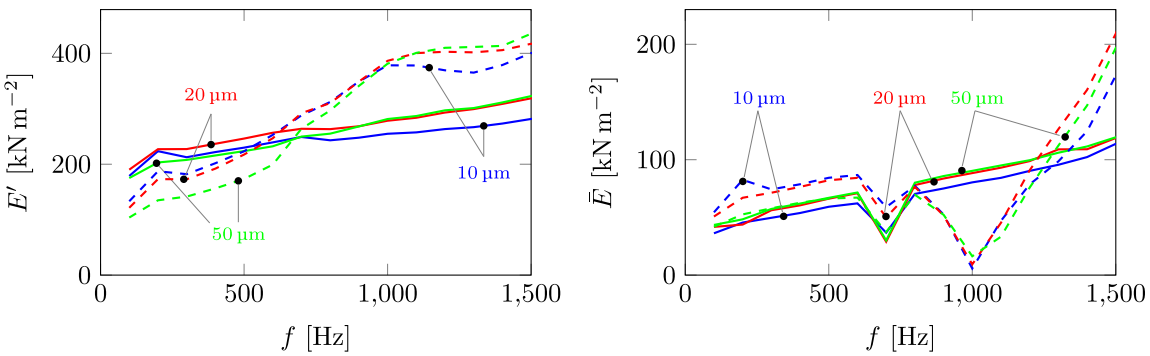

Fig. 13: Measurements with different loading amplitudes. Solid lines: Dark foam. Dashed lines: Bright foam.

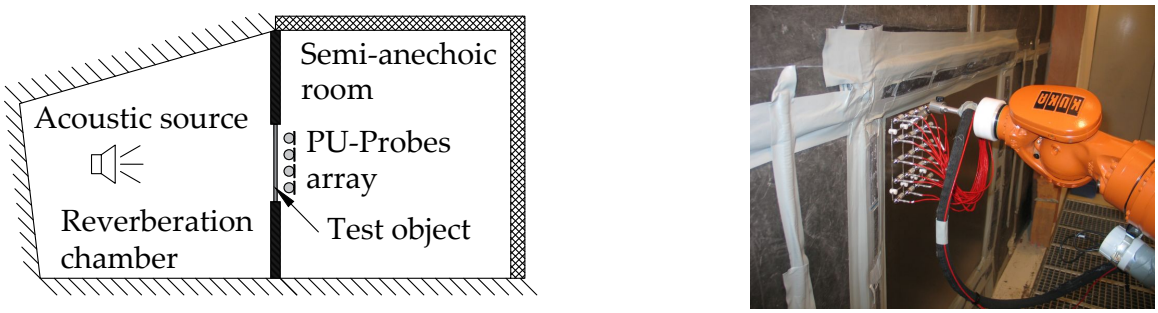

a) Schematic representation b) Scan-array with PU-probes

Fig. 14: Window test bench for transmission loss experiments.

As can be seen in Fig. 13, the increase of the loading amplitude from 10 µm to 20 µm and 50 µm has little influence on the resulting elasticity modulus. Amplitudes below 10 µm were found to be not appropriate due to the decreasing signal-to-noise ratio. Because of the limitation in the power output of the shaker, the minimal feasible loading amplitude of 10 µm is chosen in order to maximize the testable frequency range. In order to model the targeted insertion loss characteristics of the foams, the results at different initial compressions and different loading amplitudes may be extrapolated to a compression free state.

4 Application example

4.1 Window test bench as evaluation reference

In order to evaluate the accuracy of the measured frequency-dependent elasticity moduli to describe the material behaviour, several spring-mass systems were measured in a window test bench, see Fig. 14. A spring-mass system is a commonly employed noise control treatment that is formed by a poroelastic layer and a heavy layer. The system is attached to a thin steel plate, Fig. 15. This test bench is formed by two separated rooms, a reverberation chamber and a semi-anechoic room. An opening, also called window, connects the two rooms. Inside the reverberation chamber the combination of an acoustic source with the reflecting walls produces a diffuse pressure field that acts as the excitation. Hence, airborne noise transmission is investigated. In a complementary study on the acoustic behaviour of excited structures by Schrader et al. (2018), structure-borne noise was investigated. It has been determined that a frequency-dependent modelling approach achieved better results compared to constant material parameters but in a summary, no model delivered satisfactory results. This leads to the question whether alternative modelling approaches have to be pursued in order to reproduce structure-borne noise propagation.
In the connecting window the test object is placed. The basis geometry is a 1 m by 1 m steel plate of 0.75 mm thickness on which the different spring-mass systems are attached. The acoustic energy is transmitted through the object into the semi-anechoic room. The absorbing walls in this room allow an acoustic investigation under free field conditions without reflections.
The performance of the different spring-mass systems is determined by the insertion loss (IL). This quantity, commonly used in the evaluation of acoustic treatments, is defined as the difference of the sound power radiated by a bare plate Π_{rad}^{plate} and by the plate with the acoustic treatment Π_{rad}^{NCT} attached, Eq. (19).

$$\mathrm{IL}[\mathrm{dB}] = \Pi_{rad}^{plate}[\mathrm{dB}] - \Pi_{rad}^{NCT}[\mathrm{dB}] \tag{19}$$

The measurement of the radiated power was conducted with an array of PU-probes. These probes can simultaneously measure the sound pressure and sound velocity in the near field of the test object. The product of the two quantities is the sound intensity, whose integration over the complete surface results in the sound power. To facilitate the scanning process the array was installed on a robotic arm, as shown in Fig. 14 b).

4.2 Simulation model for material property evaluation

The same configuration found in the window test bench was reproduced in a numerical model, which is displayed in Fig. 15. On the basis steel plate, a diffuse pressure field is applied. This field results as the superposition of plane waves with different incident angles that are randomly determined. The total number of waves required to ensure the diffusivity of the field was previously investigated in detail by Gavila Lloret (2018). In real applications, especially on the edges of the finite plate, there is not a perfectly diffuse field. This behavior is numerically implemented by limiting the maximum incident angle of the waves to 78° (Zeller (2012)).
The remaining face of the plate is connected to the poroelastic foam layer and to the heavy layer that assemble the spring-mass system. The system radiates into the receiving fluid. In order to simulate the free radiation conditions this fluid is composed of a finite fluid volume with infinite elements on its outer layer, which is a numerical procedure to extend the domain and avoid unwanted reflections (Gavila Lloret et al. (2020)). Over this surface the total radiated power can be retrieved. The insertion loss is the quantity selected for the evaluation of the results, analogously to the measurement setup.
For the resolution with the finite element method and due to their small thickness, the steel plate and the heavy layer are discretized with solid shell elements of second order. Quadratic hexahedral elements have been employed for the discretization of the foam layer, and linear hexahedral and tetrahedral elements are chosen for the fluid domain.

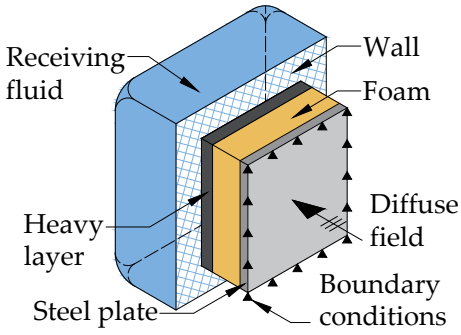

Fig. 15: Sketch of the simulation model.

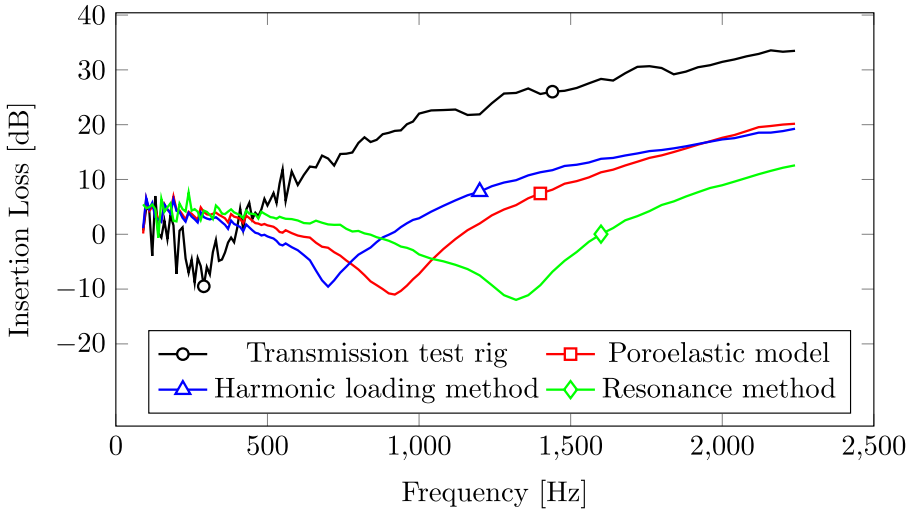

Fig. 16: Comparison of the measured and simulated insertion loss for the dark foam.

Standard values for the material properties have been applied to all components with exception to the foam, for which the properties obtained with the different characterization procedures, namely, the resonance method and the harmonic loading method, are used. It was found that the influence of the imaginary part of the elasticity modulus on the insertion loss is small and the stiffness property provided by the real part of the elasticity modulus is dominant. Regarding the resonance method, constant elasticity moduli of $E = 355.8\,\mathrm{kN/m^2} + i \cdot 43.25\,\mathrm{kN/m^2}$ for the dark foam and $E = 158.5\,\mathrm{kN/m^2} + i \cdot 68\,\mathrm{kN/m^2}$ for the bright foam were considered, based on the previous results at the highest attainable frequencies. The frequency-dependent data obtained from the harmonic loading method are indicated in Fig. 9 and Fig. 10.
In addition, the poroelastic model developed by Johnson et al. (1987); Champoux and Allard (1991) is also evaluated as reference. The required input parameters for the poroelastic model were provided by a commercial third party company. In comparison, the presented harmonic loading method for material parameter identification is easier to conduct, which is reflected in less effort in the measurement setup and implementation of the material model.
Regarding the results for the dark foam, Fig. 16, the stiffer material characterization from the resonance measuring method becomes apparent and shows that the results from the harmonic loading method are closer to the measurement results. Overall, none of the issued models meet the minimum insertion loss, which is located near 250 Hz in the experimental data. Regarding the location of the minimum, the results from the harmonic loading method show the smallest deviation. Comparing the slope of the insertion loss after the minimum qualitatively, the harmonic loading method results show the best agreement.
As can be seen from the results for the bright foam, Fig. 17, the resonance method and the harmonic loading method show a minimum in the insertion loss with approximately −2.8 dB at 420 Hz while the experimental results indicate a minimum with −1.4 dB at 240 Hz and the poroelastic model shows −4.7 dB at 480 Hz, respectively. Regarding the slope of the insertion loss, the data from the harmonic loading method shows the best agreement in the frequency range up to 1 kHz. In the frequency range above 1 kHz the slope of the poroelastic model agrees best with the experimental data.

5 Conclusion

In the present study the identification of frequency-dependent viscoelastic material parameters for two foam types was conducted. Two characterization methods with shaker test rigs were presented and their properties have been discussed. The resonance characterization method is limited regarding the evaluable frequency range, whereas the harmonic loading procedure is an economical method that delivers satisfying results for frequencies up to 2 kHz with the presented setup.
It is noted that during measurements the force sensor should be mounted on the bearing side and not on the shaker side. That way it is possible to avoid compensation calculations due to inertial forces. Furthermore, the initial loading of the foam has an influence on the resulting elasticity modulus for the foams under consideration. Therefore, an initial loading should be established in the

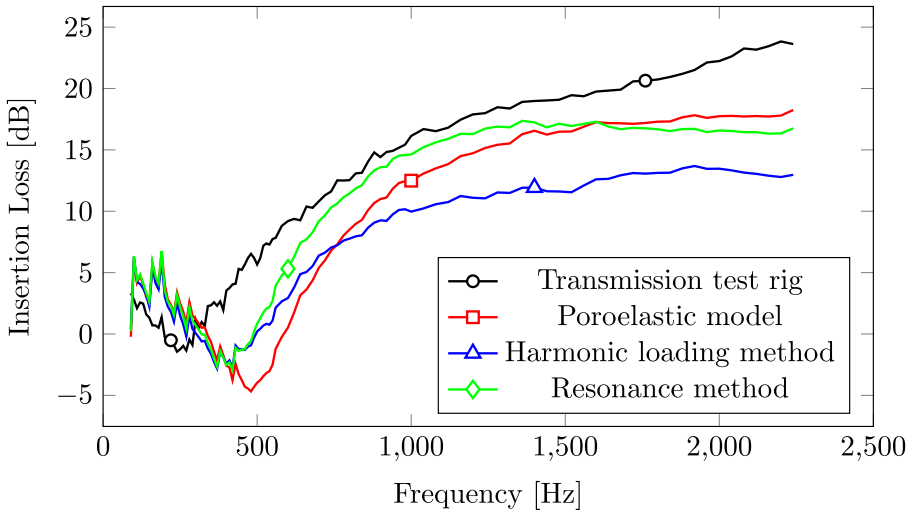

Fig. 17: Comparison of the measured and simulated insertion loss for the bright foam.

measurements which represents the final installation of the damping material.
The gained data was used in order to simulate the insertion loss achieved with the usage of the foams in spring-mass systems for noise control. The air-borne noise transmission was evaluated. From the results, the presented method in its current form is not considered sufficient for detailed insertion loss estimations but the obtained data lies in the range of the reference data, which was derived from a poroelastic simulation model and the associated parameter identification tests. In further studies it is to be considered to extend the method by samples of different shape factors in order to map possible frequency dependency of the Poisson ratio, similar to Langlois et al. (2001). As already mentioned, the method is characterized by less effort and simple implementation. The presented measurement deviations are in line with the statements made by Bonfiglio et al. (2018) regarding limited reproducibility. In order to shift resonance frequencies of the set-up out of the measuring range, the bearing mass is to be increased. Additionally, the implementation of a movable carriage to position the shaker more precisely should be considered.

Acknowledgement

The second author is a member of the joint project “Kompetenzzentrum eMobility - KeM”, which is financially supported by the European Union and the German State of Saxony-Anhalt. This support is gratefully acknowledged.

References

J. F. Allard and G. Daigle. Propagation of sound in porous media: Modeling sound absorbing materials. *J. Acoust. Soc. Am.*, 95: 2785–2785, 1994. ISSN 0001-4966. doi: 10/cs5gbg.

J. F. Allard, G. Jansens, G. Vermeir, and W. Lauriks. Frame-borne surface waves in air-saturated porous media. *J. Acoust. Soc. Am.*, 111(2):690–696, 2002. doi: 10/bjkdbf.

J. F. Allard, M. Henry, L. Boeckx, P. Leclaire, and W. Lauriks. Acoustical measurement of the shear modulus for thin porous layers. *J. Acoust. Soc. Am.*, 117(4):1737–1743, 2005. doi: 10/b8cpds.

Y. Atalla and R. Panneton. Inverse acoustical characterization of open cell porous media using impedance tube measurements. *Canadian Acoustics*, 33(1):11–24, 2005. ISSN 2291-1391.

M. A. Biot. Theory of propagation of elastic waves in a fluid-saturated porous solid. i. low-frequency range. *J. Acoust. Soc. Am.*, 28(2):168–178, 1956a. doi: 10/dw58r8.

M. A. Biot. Theory of propagation of elastic waves in a fluid-saturated porous solid. ii. higher frequency range. *J. Acoust. Soc. Am.*, 28(2):179–191, 1956b. doi: 10/dv5c7p.

L. Boeckx, P. Leclaire, P. Khurana, C. Glorieux, W. Lauriks, and J. F. Allard. Investigation of the phase velocities of guided acoustic waves in soft porous layers. *J. Acoust. Soc. Am.*, 117(2):545–554, 2005. doi: 10/dq2ghs.

P. Bonfiglio and F. Pompoli. Determination of the dynamic complex modulus of viscoelasticmaterials using a time domain approach. *Polymer Testing*, 48:89–96, 2015. doi: 10/f744cp.

P. Bonfiglio et al. How reproducible are methods to measure the dynamic viscoelastic properties of poroelastic media? *J. Sound Vib.*, 428:26–43, 2018. doi: 10/c53q.

Y. Champoux and J. F. Allard. Dynamic tortuosity and bulk modulus in air-saturated porous media. *J. Appl. Phys.*, 70:1975–1979, 1991. ISSN 0021-8979. doi: 10/d2fgwv.

J. Cuenca, C. Van der Kelen, and P. Göransson. A general methodology for inverse estimation of the elastic and anelastic properties of anisotropic open-cell porous materials – with application to a melamine foam. *J. Appl. Phys.*, 115(8):084904, 2014. doi: 10/f23f73.

F. Duvigneau and S. Duczek. A numerical study on the potential of acoustic metamaterials. In H. Altenbach, E. Carrera, and G. Kulikov, editors, *Analysis and Modelling of Advanced Structures and Smart Systems*, Advanced Structured Materials, pages 11–34. Springer, 2017. doi: 10/c2tc.

F. Duvigneau, S. Nitzschke, E. Woschke, and U. Gabbert. A holistic approach for the vibration and acoustic analysis of combustion engines including hydrodynamic interactions. *Arch. Appl. Mech.*, 86:1887–1900, 2016. doi: 10/f89p87.

J. D. Ferry. *Viscoelastic Properties of Polymers*. Wiley-Blackwell, 1980. ISBN 0471048941.

S. Finnveden, N. E. Hörlin, and M. Barbagallo. Dynamic characterization of viscoelastic porous foams used in vehicles based on an inverse finite element method. *J. Acoust. Soc. Am.*, 135(4):1834–1843, 2014. doi: 10/f22t2d.

M. Gavila Lloret. *Prediction of the airborne sound transmission through a car front end model including poroelastic acoustic treatments*. PhD thesis, Otto von Guericke University Magdeburg, 2018.

Maria Gavila Lloret, Gregor Müller, Fabian Duvigneau, and Ulrich Gabbert. On the numerical modeling of poroelastic layers in spring-mass systems. *Applied Acoustics*, 157:106996, 2020. doi: 10/ggj3zj.

L. Jaouen, A. Renault, and M. Deverge. Elastic and damping characterizations of acoustical porous materials: Available experimental methods and applications to a melamine foam. *Appl. Acoust.*, 69(12):1129–1140, 2008. doi: 10/c57kcv.

D. L. Johnson, J. Koplik, and R. Dashen. Theory of dynamic permeability and tortuosity in fluid-saturated porous media. *J. Fluid Mech.*, 176:379, 1987. ISSN 0022-1120. doi: 10/bm7st4.

D. Koblar and M. Boltežar. Evaluation of the frequency-dependent Young's modulus and damping factor of rubber from experiment and their implementation in a finite-element analysis. *Exp. Tech.*, 40(1):235–244, 2016. doi: 10/f86svc.

R. S. Lakes. *Viscoelastic solids*. CRC press, 1998. ISBN 9780849396588.

C. Langlois, R. Panneton, and N. Atalla. Polynomial relations for quasi-static mechanical characterization of isotropic poroelastic materials. *J. Acoust. Soc. Am.*, 110(6):3032–3040, 2001. doi: 10/b2wqck.

R. Lerch, G. Sessler, and D. Wolf. *Technische Akustik*. Springer-Verlag Berlin Heidelberg, 2009.

A. D. Nashif, D. I. Jones, and J. P. Henderson. *Vibration Damping*. John Wiley & Sons, Inc., 1985. ISBN 9780471867722.

S. R. Pride and J. G. Berryman. Connecting theory to experiment in poroelasticity. *J. Mech. Phys. Solids*, 46(4):719–747, 1998. doi: 10/dqfj2p.

T. Pritz. Frequency dependence of frame dynamic characteristics of mineral and glass wool materials. *J. Sound Vib.*, 106(1): 161–169, 1986. doi: 10/cf5rfr.

T. Pritz. Dynamic Young's modulus and loss factor of plastic foams for impact sound isolation. *J. Sound Vib.*, 178(3):315–322, 1994. doi: 10/dfbs9n.

A. Renault. *Caractérisation mécanique dynamique de matériaux poro-viscoélastiques (Dynamic mechanical characterization of poro-visco-elastic materials)*. PhD thesis, Université de Sherbrooke, 2008.

S. Rigobert, F. C. Sgard, and N. Atalla. A two-field hybrid formulation for multilayers involving poroelastic, acoustic, and elastic materials. *J. Acoust. Soc. Am.*, 115(6):2786–2797, 2004. doi: 10/cpgtqz.

Y. Salissou and R. Panneton. Pressure/mass method to measure open porosity of porous solids. *J. Appl. Phys.*, 101:124913, 2007. ISSN 0021-8979. doi: 10/frm5hg.

P. Schrader, F. Duvigneau, M. Gavila Lloret, H. Rottengruber, and U. Gabbert. Finite element analysis of the acoustic behavior of poroelastic materials based on experimentally determined frequency-dependent material properties. In *28th edition of the Biennial ISMA conference on Noise and Vibration Engineering*, Leuven, 2018.

A. Sfaoui. On the viscoelasticity of the polyurethane foam. *J. Acoust. Soc. Am.*, 97(2):1046–1052, 1995. doi: 10/bspvtm.

C. Van der Kelen, P. Göransson, B. Pluymers, and W. Desmet. On the influence of frequency-dependent elastic properties in vibro-acoustic modelling of porous materials under structural excitation. *J. Sound Vib.*, 333(24):6560–6571, 2014. doi: 10/f22tf6.

P. Zeller. *Handbuch Fahrzeugakustik*, volume 2. Vieweg+Teubner Verlag, Wiesbaden, Springer, 2012.